Journal of Alloys and Compounds 509 (2011) 372–379

Contents lists available at ScienceDirect

Journal of Alloys and Compounds

journal homepage: www.elsevier.com/locate/jallcom

Hydrogenation properties of Fe–Ti–V bcc alloys

B. Massicot, M. Latroche*, J.-M. Joubert

CNRS, ICMPE-CMTR, UMR7182, 2-8 rue Henri Dunant, 94320 Thiais, France

ARTICLE INFO

Article history:
Received 26 July 2010
Received in revised form 2 September 2010
Accepted 3 September 2010
Available online 16 September 2010

Keywords:
Types of material: hydrogen absorbing materials
Metal hydrides
Preparation and processing: gas–solid reactions
Phenomena: crystal structure
Enthalpy
Thermodynamic properties

ABSTRACT

The hydrogenation properties of Fe–Ti–V bcc alloys have been studied by the Sieverts method. Starting from a fully determined ternary phase diagram, a large number of compositions have been synthesized and pressure–composition–isotherms have been measured at different temperatures both in the low and high hydrogen concentration regions. The enthalpies of absorption and desorption have been found to vary linearly as a function of composition in the ternary domain and depend on the ones of the pure elements. The absorption capacity is mainly dependent on the iron concentration. Additionally, the crystal structure of the hydrides has been studied. For the first time a progressive and continuous distortion from body centered cubic (bcc) to body centered tetragonal (bct) structure has been evidenced.

1. Introduction

Vanadium-based hydrogen absorbing alloys with body centered cubic (bcc) structure show promising weight capacities compared to rare earth based storage materials because of the relatively low atomic mass of vanadium. Indeed, conventional metal hydrides have weight capacities less than 1.8 wt% whereas Ti–V based solid solutions exhibit a total capacity close to 4 wt% [1]. Hydrogenation of the bcc alloys occurs via the successive formation of two hydrides, the first one being unfortunately too stable to give rise to reversible storage [2,3]. However, the second hydride is less stable and hydrogen absorption or desorption can be carried out close to ambient conditions with a reversible capacity limited to the difference of hydrogen concentration in the first and the second hydride. From the kinetic point of view, rapid reactions with hydrogen occur at room temperature only with bcc phases in which small amounts of a third element with atomic radius 5% smaller than titanium have been added [4]. Thus substitutions of Ti–V alloys by 3*d* transition elements are usually investigated to improve the hydrogenation behavior. Many works have been dedicated to the Cr–Ti–V system which shows a reversible capacity of 2.4 wt% at room temperature [10–12,5–9] whereas other studies report on the hydrogenation behavior of *M*–Ti–V compounds with *M* = Mn, Fe, Co, Ni [13–17,2]. Iron-containing alloys were found to present good reversible capacity among these systems. Lynch et al. [18] have shown that for $(V_{0.9}Ti_{0.1})_{1-x}Fe_x$, varying x from 0 to 0.075 allows to change the plateau pressure within more than one order of magnitude without affecting capacity. Moreover, as the high cost of vanadium is one of the main drawbacks limiting the practical application of bcc alloys, the possibility to use cheaper ferrovanadium alloys is of peculiar interest [19–22].

Maeland et al. [18,2,23–25,3,4] studied the hydrogenation properties of the bcc Fe–Ti–V alloys in the composition ranges $(Ti_{0.1}V_{0.9})_{1-x}Fe_x$, $0 < x < 0.075$ and $(V_{1-y}Ti_y)_{0.98}Fe_{0.02}$, $y = 0.1, 0.2$ and 0.25. The maximal hydrogen concentration reaches 2 H/M, with a pressure plateau between 1 and 2 H per metal atom (H/M). Nomura and Akiba [14] investigated the Fe–Ti–V system in the composition range Ti(33–47 mol%)–V(42–67 mol%)–Fe(0–14 mol%) and found that the best composition for hydrogen absorption was $Ti_{43.5}V_{49.0}Fe_{7.5}$ with a maximum hydrogen uptake of 3.90 wt% (H/M = 1.90) at 253 K and a reversible capacity of 2.4 wt% when hydrogenated at 253 K and desorbed at 573 K under 1 atm. Kagawa et al. [26] studied the thermodynamic properties of hydrogen desorption for slightly higher titanium rates, and Challet et al. [27] measured absorption–desorption isotherms for $(Ti_{0.35}V_{0.65})_{1-x}Fe_x$, $x = 0.07$ and 0.14. A comparison of these works shows that the addition of iron to a Fe–Ti–V alloy destabilizes the hydride, while an increase of the titanium concentration stabilizes it. Apart from the results of Nomura and Akiba [14] and Challet et al. [27], few thermodynamic data were harvested for iron contents higher than 7.5 at.%.

* Corresponding author. Tel.: +33 1 49 78 12 10; fax: +33 1 49 78 12 03.
E-mail addresses: michel.latroche@icmpe.cnrs.fr, latroche@glvt-cnrs.fr (M. Latroche).

0925-8388/$ – see front matter © 2010 Elsevier B.V. All rights reserved.
doi:10.1016/j.jallcom.2010.09.030

Table 1
Phase analysis of the metallic samples, after annealing at 1000 °C. All samples are single bcc phase.

Sample no.	Nominal composition	Measured composition (at.%)		Lattice parameter	
		Ti	V	Fe	a (nm)
0	$Ti_{10}V_{80}Fe_{10}$[a]	10.2(7)	80.2(2)	9.6(6)	0.30223(4)
1	$Ti_{10}V_{88}Fe_2$	9.8(3)	88.3(4)	1.9(1)	0.30447(3)
2	$Ti_{12}V_{70}Fe_{18}$[a]	11.7(2)	71.2(3)	17.2(2)	0.30017(7)
3	$Ti_{20}V_{70}Fe_{10}$	20.4(3)	69.8(4)	9.7(2)	0.30479(3)
4	$Ti_{20}V_{78}Fe_2$	20.6(7)	77.4(7)	2.0(1)	0.30720(3)
5	$Ti_{30}V_{50}Fe_{20}$[b]	29.2(1)	50.7(2)	20.1(1)	0.30379(9)
6	$Ti_{30}V_{60}Fe_{10}$	31.1(2)	58.9(2)	10.0(1)	0.30738(7)
7	$Ti_{40}V_{50}Fe_{10}$	40.9(1)	48.9(1)	10.2(1)	0.30980(4)
8	$Ti_{41}V_{41}Fe_{18}$	42.1(1)	41.0(1)	16.9(1)	0.30808(5)
9	$V_{90}Fe_{10}$[a]	–	90.8(8)	9.2(8)	0.29981(4)

[a] The maximal concentration of absorbed hydrogen did not exceed 1 H/M.
[b] Annealed at 1200 °C.

Recently, we investigated the ternary phase diagram of the Fe–Ti–V system at 1000 °C, in order to precisely determine the extension of the bcc domain [28]. We also studied the influence of the annealing temperature by measuring the isothermal section at 1200 °C. We found that 15 at.% Fe can be substituted in the bcc Ti–V solid solution at both temperatures and we have shown that the lattice parameters of the bcc phase depends linearly on the composition. In the present work, with the help of these phase diagram data, we report on the hydrogenation properties (equilibrium pressure, total and reversible capacity) of Fe–Ti–V alloys over a larger composition range in the bcc domain. We found that enthalpies of absorption and desorption vary linearly as a function of composition in agreement with previous finding but extended here to a larger composition domain. The structural changes during hydrogen absorption are also investigated.

2. Experimental details

The alloys (5 g) were synthesized by melting the pure bulk metals (99.98% Fe from Sigma Aldrich, 99.99% Ti from Alfa Aesar, 99.9% V from Goodfellow) in a cold crucible induction furnace under argon atmosphere. Each alloy was turned over and melted four times to ensure a good homogeneity. The obtained samples were annealed for three weeks at 1000 °C or 1200 °C in a resistive furnace. Before annealing, the samples were wrapped in a tantalum foil and introduced into a silica tube evacuated to high vacuum, filled with argon so that the inner pressure would be 1 bar at the annealing temperature and sealed. Tantalum prevents contamination from the silica. After annealing, the alloys were quenched by dropping the silica tube into water. Weight losses during melting were not detectable. Typical weight losses during heat treatment were less than 0.5%.

X-ray diffraction (XRD) experiments were performed at room temperature on a Bruker AXS D8 θ–θ diffractometer using Cu-K_α radiation (λ = 1.5418 Å, Bragg-Brentano geometry, 2θ-range 20–120°, step size 0.04°, in beam rear graphite monochromator). The lattice parameters were refined with the Rietveld method [29] using the program FullProf [30]. The uncertainty on the lattice parameters was calculated by multiplying the standard deviation given by the FullProf program by the Bérar factor [31,32]. The chemical composition of the phases was investigated on bulk samples by electron probe microanalysis (EPMA) with a CAMECA SX100. Acceleration voltage and beam current were 15 kV and 40 nA, respectively. The composition of the alloys was determined from 10 to 100 measurements; the standard deviation of these measurements is given as the uncertainty on the phase composition and results from counting statistics, the experimental setup and alloy homogeneity.

The samples (0.5 g) were hydrogenated by exposing them to pure gaseous hydrogen (99.9999% H_2 from Alphagaz). The sample surface was first filed under argon atmosphere in order to eliminate possible surface oxides, and the sample was introduced in the sample holder under argon atmosphere. The activation of the hydrogenation reaction was performed by exposing the sample to 25 bar H_2 at room temperature, then heating it at 500 °C under vacuum for 1 h, and then cooling down back to room temperature. This cycle was repeated four times, after which the sample was considered to be activated. Such treatment was performed in order to ensure fully activated samples but further studies [33] have shown that these bcc samples can also be activated in milder conditions at room temperature.

Pressure–Composition–Isotherm (PCI) curves at different temperatures were then measured by the manometric Sieverts method [34] using different pressure gauges (1, 10 and 100 bar) according to the measuring ranges. The uncertainty on the measured hydrogen concentrations in the metals is about 10% of the fully charge capacity (i.e. 0.2 H/M max.) and the pressure accuracy is about 0.1% of the full scale (i.e. 0.1 bar max).

3. Results

The hydrogenation properties were studied for ten metallic compositions inside the bcc domain. According to our ternary phase diagram [28] an annealing temperature of 1000 °C was enough to obtain bcc single phased samples for every composition but $Ti_{50}V_{30}Fe_{20}$. For this latter composition, again according to the phase diagram [28], a single phase sample could be obtained by treating the sample at 1200 °C. Table 1 summarizes the measured compositions and structural properties of each studied samples after annealing.

It is worth to note that annealing treatment was performed in order (i) to have fully equilibrated sample and (ii) to obtain increasing amount of dissoluted iron in the bcc phase by raising the annealing temperature. However, this does not preclude the possibility of using non-annealed sample. Indeed, in a recent work to be published elsewhere [33] it was demonstrated that the hydrogenation properties of an as-cast bcc sample with composition $Ti_{24.5}V_{59.3}Fe_{16.2}$ does not need annealing nor pretreatment to be hydrogenated though for the first hydrogenation, the kinetic is found to be slightly slower and the plateau pressures slightly higher for the as-cast alloy than for the annealed sample.

As mentioned in Section 1, the hydrogenation of the bcc alloys involves the successive formation of two hydrides [2,3]. The first hydride is usually stable and is observed around 1 H/M whereas the second exists for values close to 2 H/M. Accordingly, the present study will be divided into two parts addressing the phases observed in the PCI curve above and below 0.9 H/M, respectively.

Table 2
Maximum capacity measured during activation (25 °C, 2.5 MPa) for samples 0, 2 and 9.

Sample no.	Nominal composition	Maximum capacity (±0.1 H/M)
0	$Ti_{10}V_{80}Fe_{10}$	0.97
2	$Ti_{12}V_{70}Fe_{18}$	0.95
9	$V_{90}Fe_{10}$	0.95

3.1. Capacity above 0.9 H/M

Among the studied samples, $Ti_{10}V_{80}Fe_{10}$, $Ti_{12}V_{70}Fe_{18}$ and $V_{90}Fe_{10}$, i.e. sample nos. 0, 2 and 9, did not absorb more than 1 H/M (Table 2) at room temperature. Moreover, the PCI curves of these samples could not be measured properly because of poor reproducibility and a rapid drop of the maximum hydrogen storage capacity after few cycles.

The PCI curves of every other sample (nos. 1 and 3–8) were measured at different temperatures ranging between 25 and 200 °C depending on the equilibrium pressures and are shown in Fig. 1. Each obtained PCI curve in the hydrogen rich region (>0.9 H/M) presents a plateau, with a significant hysteresis and a slight slope. As already stated, the hydrogen poor region cannot be measured by the Sieverts method in this temperature range due to very low equilibrium pressure.

From the determination of the plateau pressure at different temperatures, it is possible to calculate the enthalpy of formation and dissociation of the hydride for each alloy from the van't Hoff equation. To be accurate, the determination of both parameters requires data points in a wide range of temperature. In our case, due to the limited investigated temperature range, we chose to refine the only enthalpy keeping the entropy to 130 $J\,K^{-1}\,mol(H_2)^{-1}$, a value commonly accepted as the entropy of gaseous hydrogen. The results obtained by this method are reported in Table 3. In addition, the values of the plateau pressure at 100 °C for absorption and desorption are also given in this table.

In Table 4, other characteristics of the measured isotherms are given: maximal capacity (at 25 °C, 10 bar), plateau widths, hysteresis factor $\log(P_{abs}/P_{des})$ at 25 °C and plateau slope $d(\log P)/d(H/M)$.

3.2. Capacity below 0.9 H/M

The equilibrium pressures at room temperature for hydrogen concentrations smaller than 0.9 H/M are lower than 10^{-3} bar and thus difficult to measure with a classical Sieverts apparatus. It was consequently not possible to determine whether a pressure plateau exists at this temperature in this concentration region. However, by increasing the temperature above 100 °C, it is possible to raise significantly the pressure to obtain measurable PCI curves for the low hydrogen concentration domain. These measurements have been done for three samples $Ti_{10}V_{88}Fe_2$ (no. 1); $Ti_{20}V_{70}Fe_{10}$ (no. 3) and $Ti_{41}V_{41}Fe_{12}$ (no. 8). The PCI curves at temperatures between 150 °C and 350 °C are presented in Fig. 2. The isotherms present neither hysteresis nor plateau. That indicates that this range of hydrogen concentration and temperature is characterized by a single phase solid solution domain rather than the coexistence of two phases, one poor and one rich in hydrogen as observed for the region above 0.9 H/M. However, these measurements do not preclude the appearance of a pressure plateau at lower temperature.

To answer this question, the $Ti_{20}V_{70}Fe_{10}$ sample (no. 3) was further investigated by room temperature XRD after loading at different hydrogen concentrations. Fig. 3 presents the evolution of the obtained diffraction patterns as a function of the hydrogen content. As previously reported, the alloy $Ti_{20}V_{70}Fe_{10}$ adopts a bcc structure at 0 H/M. For higher hydrogen concentrations, a splitting of the diffraction peaks takes place and the patterns cannot be indexed in a simple bcc structure. Some authors report on the possible formation of a body centered tetragonal (bct) phase upon hydrogenation [35–37]. This structure adopts the space group $I4_1/amd$ and can be described as a superstructure of the bcc phase with $\boldsymbol{a}_{bct} = 2\cdot\boldsymbol{a}_{bcc}$ and $\boldsymbol{c}_{bct} = 2\cdot\boldsymbol{a}_{bcc}$. The metallic atoms lying in site 2*a* (0,0,0) in the bcc cubic cell occupy site 16 *h* (*x*,0,*z*) with $x = \frac{1}{4}$ and $z = \frac{3}{8}$ in the bct cell. Several possibilities were used to refine the patterns: (i) coexistence of a bcc and a body centered tetragonal phase, (ii) coexistence of two bcc phases, or (iii) a single bct phase. For each concentration higher than 0 H/M, the single bct phase leads to the best refinement. Therefore it was considered that the structure is submitted to a progressive and continuous tetragonal distortion when the hydrogenation concentration increases from 0 to 0.87 H/M. It is worth to note that the lattice parameter *a* remains nearly constant whereas *c* increases linearly as a function of the hydrogen concentration (Fig. 4).

The evolution of the cell volume per metal atom as a function of the hydrogen concentration is shown in Fig. 5. It increases linearly between 0 and 0.87 H/M. For the sake of comparison, the cell volume for the fully charged hydride at 1.76 H/M, for which the structure is face centered cubic (fcc), is also shown in Fig. 5. One can see that this point is located slightly above a straight line that could be extrapolated from the lower hydrogen concentrations. This indicates that the discontinuous phase transformation taking place between 0.87 and 1.76 H/M induces a larger increase of the cell volume per additional hydrogen uptake than the continuous transformation for hydrogen concentrations lower than 0.87 H/M.

4. Discussion

To correlate the thermodynamic data observed for the hydrogen rich part (>0.9 H/M) to the structural data, the desorption pressures obtained at 100 °C have been plotted versus the cell volume of the alloys before hydrogenation in Fig. 6. One can see that it exists a linear relationship between the two parameters and accordingly that the size effect is the major factor controlling the thermodynamic properties for this alloy family as already reported for other substituted systems like Ti–V [26] or $LaNi_5$ [38].

It was established in previous work [28] that the lattice parameters of the alloys depend linearly on the composition following the relationship:

$$a = 0.3281 \cdot x\mathrm{Ti} + 0.3027 \cdot x_V + 0.2703 \cdot x\mathrm{Fe} \quad (1)$$

Cell volume and lattice parameters have a cubic dependence but an almost linear relationship can be assumed within the limited investigated composition range. In addition, the pressure logarithm and the enthalpy are related by:

$$\mathrm{Ln}(P) = \frac{\Delta H}{RT} - \frac{\Delta S}{R} \quad (2)$$

and a constant entropy as a function of the composition and temperature is assumed (see Section 3.1). It is therefore possible to model the formation and dissociation enthalpies of the hydride as a function of the metallic composition of the Fe–Ti–V system. Indeed, over the studied composition range, a linear relationship describes fairly well the behavior of the system using the following equations:

$$\Delta H_{abs} = -102 \cdot x_{Ti} - 36 \cdot x_V + 73 \cdot x_{Fe} \quad (3)$$

$$\Delta H_{des} = 117 \cdot x_{Ti} + 38 \cdot x_V - 80 \cdot x_{Fe} \quad (4)$$

where ΔH_{abs} and ΔH_{des} are respectively the enthalpies of formation and decomposition of the dihydride, in $kJ\,mol(H_2)^{-1}$ and x_{Ti},

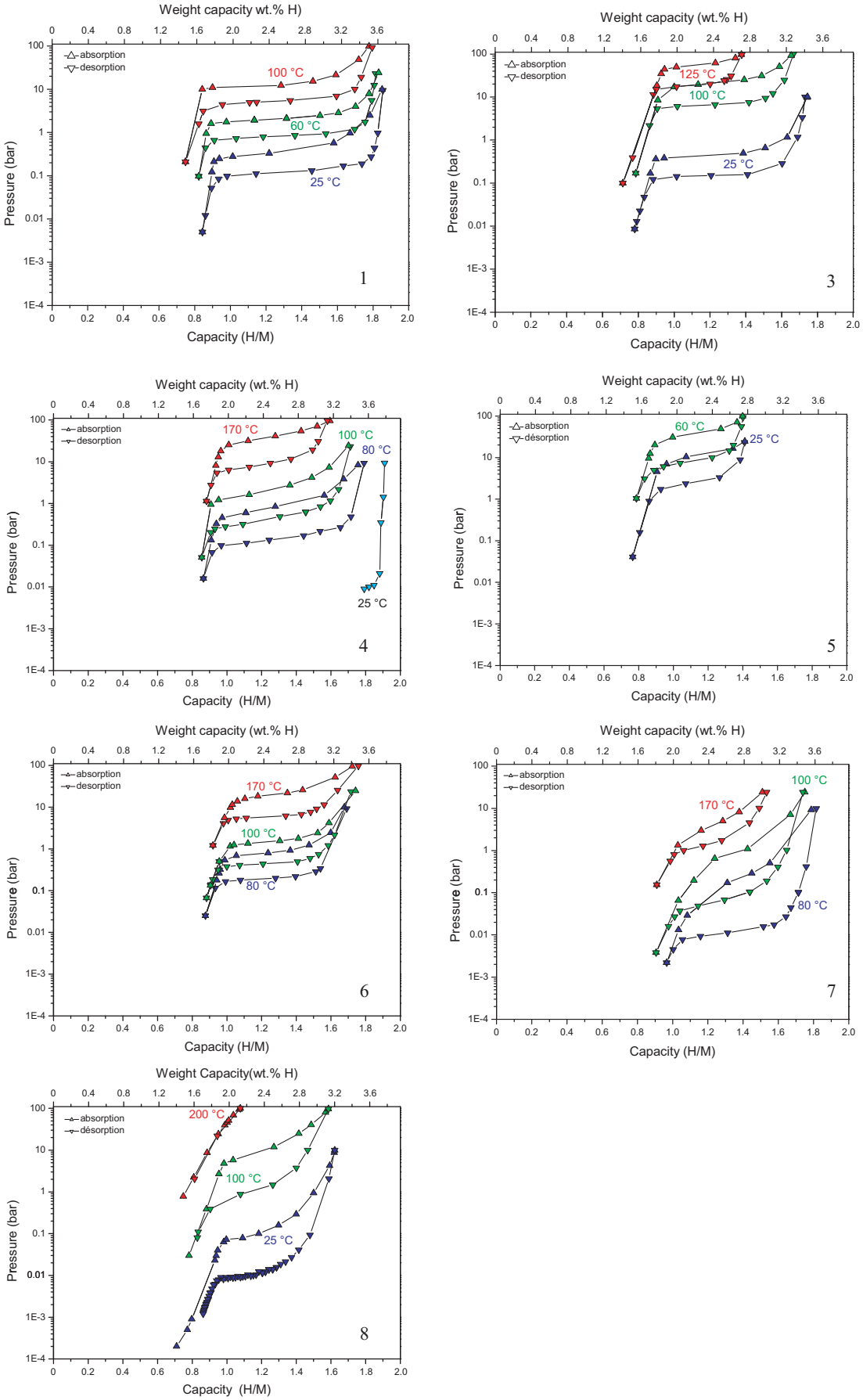

Fig. 1. Pressure–Composition–Isotherm curves of sample nos. 1, 3–8 (see Table 1 for detailed compositions) at temperatures ranging from 25 to 200 °C in the hydrogen rich region (>0.9 H/M) (maximum error bars: ±0.2 H/M and ±0.1 bar).

Table 3
Absorption and desorption thermodynamic data of the studied samples. The ΔH° values are calculated assuming $\Delta S^\circ = 130\,J\,K^{-1}\,mol(H_2)^{-1}$. The plateau pressures at 100 °C are also reported (abs: absorption; des: desorption).

Sample no.	Nominal composition	ΔH° for fixed ΔS° (kJ mol$(H_2)^{-1}$)		$P_{plateau}$ at 100 °C (±0.1 bar)	
		abs	des	abs	des
1	$Ti_{10}V_{88}Fe_2$	−41	44	13	5.4
3	$Ti_{20}V_{70}Fe_{10}$	−40	43	22	6.6
4	$Ti_{20}V_{78}Fe_2$	−46	51	2.3	0.45
5	$Ti_{30}V_{50}Fe_{20}$	−33	37	112[a]	24[a]
6	$Ti_{30}V_{60}Fe_{10}$	−47	51	1.5	0.45
7	$Ti_{40}V_{50}Fe_{10}$	−52	57	0.48	0.069
8	$Ti_{41}V_{41}Fe_{18}$	−44	50	8.1	1.1

[a] Extrapolated at 100 °C from the measurements at other temperatures.

Table 4
Maximum capacity, plateau width, hysteresis factor, plateau slope for the absorption/desorption isotherms measured above 0.9 H/M at 25 °C.

Sample no.	Nominal composition	Maximal capacity (±0.2 H/M)	Plateau width (±0.2 H/M)	Hysteresis factor (±0.01)	Plateau slope (±0.01)
1	$Ti_{10}V_{88}Fe_2$	1.86	0.83	0.39	0.24
3	$Ti_{20}V_{70}Fe_{10}$	1.74	0.70	0.52	0.26
4	$Ti_{20}V_{78}Fe_2$	1.91	0.72	0.71	0.77
5	$Ti_{30}V_{50}Fe_{20}$	1.41	0.43	0.65	0.76
6	$Ti_{30}V_{60}Fe_{10}$	1.69	0.58	0.51	0.27
7	$Ti_{40}V_{50}Fe_{10}$	1.81	0.60	0.84	1.20
8	$Ti_{41}V_{41}Fe_{18}$	1.62	0.38	0.89	–

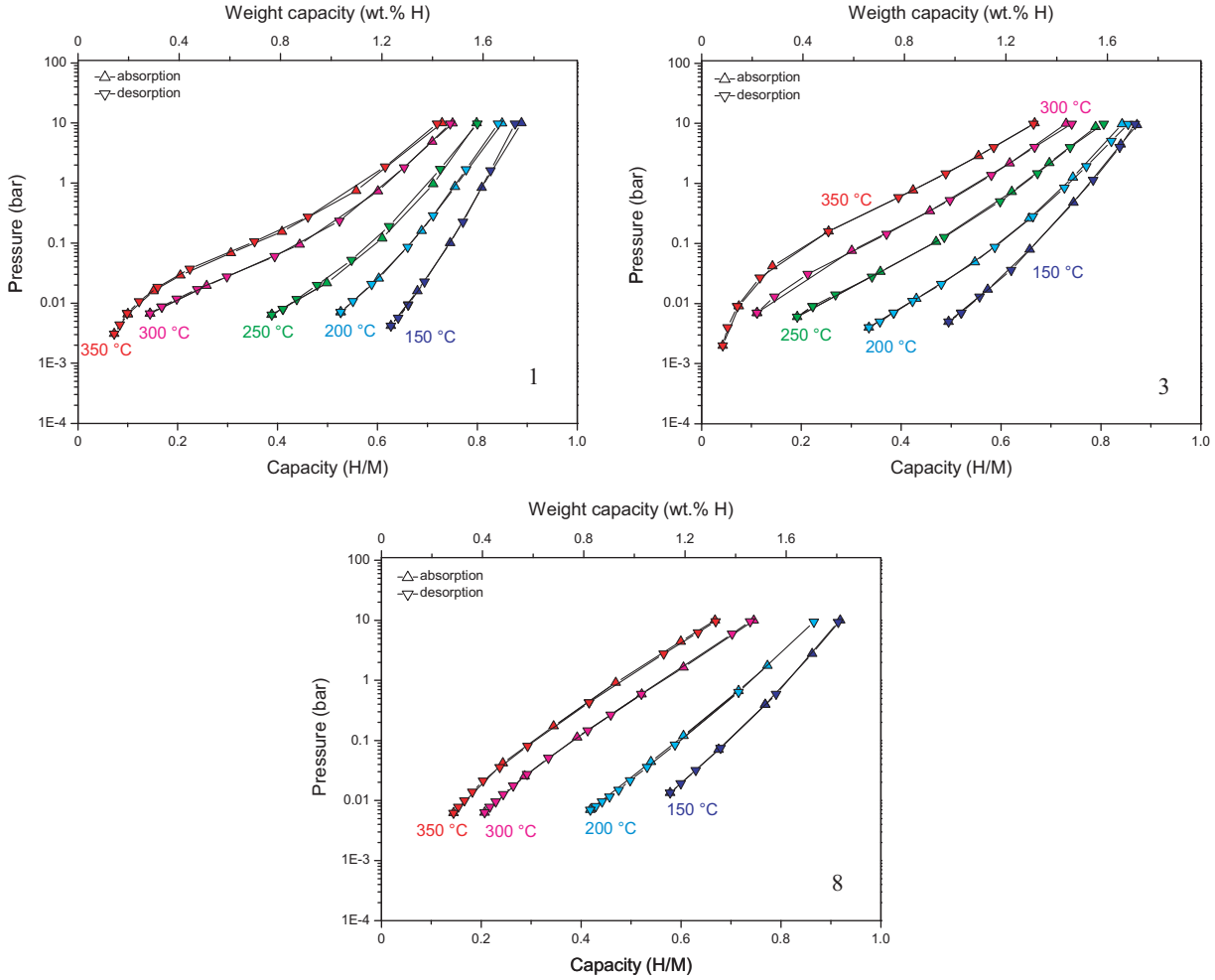

Fig. 2. Pressure–composition isotherms of the samples $Ti_{10}V_{88}Fe_2$ (no. 1); $Ti_{20}V_{70}Fe_{10}$ (no. 3) and $Ti_{41}V_{41}Fe_{12}$ (no. 8) measured in the temperature range between 150 °C and 350 °C for hydrogen concentrations smaller than 0.9 H/M (maximum error bars: ±0.2 H/M and ±0.1 bar).

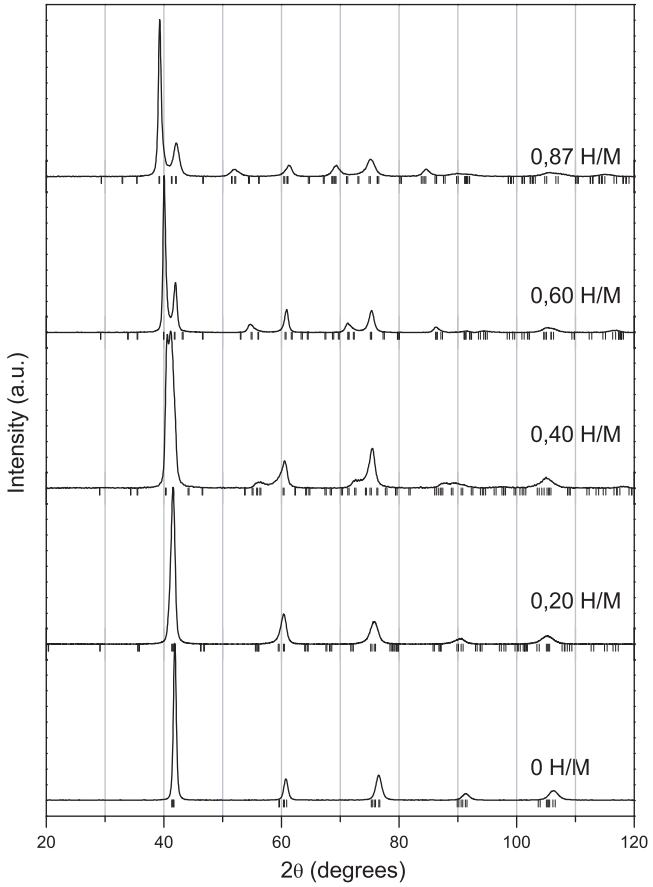

Fig. 3. Room temperature X-ray diffration diagrams of sample $Ti_{20}V_{70}Fe_{10}$ (no. 3) for different hydrogen concentrations. For 0 H/M the structure is bcc and for concentration higher than 0 H/M, the structure is bct with $a_{bct} = 2 \cdot a_{bcc}$ and $c_{bct} = 2 \cdot a_{bcc}$ (see text for details).

x_V and x_{Fe} are the molar fractions of titanium, vanadium and iron in the hydrogen-free compound, respectively.

The reliability factors for the linear interpolations leading to Eqs. (3) and (4) are $R^2 = 0.9994$ for absorption and 0.9997 for desorption. The average difference is less than 0.8 kJ mol$(H_2)^{-1}$ between our measured and calculated data and less than 4 kJ mol$(H_2)^{-1}$ between

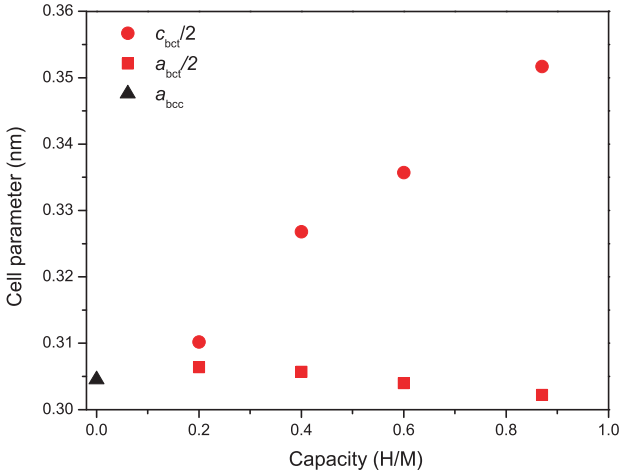

Fig. 4. Evolution of the cell parameters of the sample $Ti_{20}V_{70}Fe_{10}$ (no. 3) as a function of the hydrogen content in the low concentration region (<0.9 H/M). For sake of comparison with the bcc phase, the cell parameters of the bct phase have been divided by a factor of two (maximum error bars: ±0.2 H/M, ±0.1 bar and ±0.0001 nm).

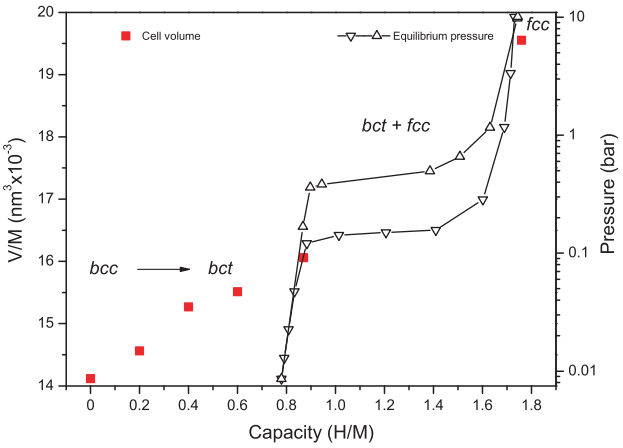

Fig. 5. Evolution oft the cell volume reduced to one metal atom as a function of the hydrogen concentration, for the sample $Ti_{20}V_{70}Fe_{10}$ (no. 3). The pressure–composition isotherm at 25 °C has also been plotted (maximum error bars: ±0. 2 H/M, ±0.1 bar and $\pm 0.065 \times 10^{-3}$ nm^3).

our calculated data and those reported in [2,3]. In Eq. (4), the coefficients associated with molar fractions can be seen as the partial desorption enthalpies of the pure elements for the formation reaction between MH and MH_2. Table 5 provides a comparison of these values with the enthalpies of desorption of the pure elements.

We observe that the values for vanadium are very close, which is not surprising since this element is the major constituent of our samples. The values for titanium [39] remain relatively close, with a difference of 19 kJ mol$(H_2)^{-1}$. Finally a difference of 60 kJ mol$(H_2)^{-1}$ is obtained for iron between the partial enthalpy and enthalpy of desorption of pure metal. This large difference can be explained by the fact that the value from the literature [39] stands for the reaction between Fe and $FeH_{0.5}$ and does not involve the FeH_2 hydride, as it is the case for the other elements. According to Eqs. (3) and (4), it can be concluded that the addition of iron destabilizes the hydride, while addition of titanium stabilizes it. Considering that iron hydride is less stable than the vanadium hydride, which in turn is less stable than the titanium hydride, it can be derived that the combination of the different elements into a bcc Fe–Ti–V alloy is in agreement with the relative hydrogenation properties of the pure constitutive elements. This can be better visualized in Fig. 7, in which has been plotted lines corresponding to equal values of the enthalpy of formation of the hydride in the ternary phase diagram.

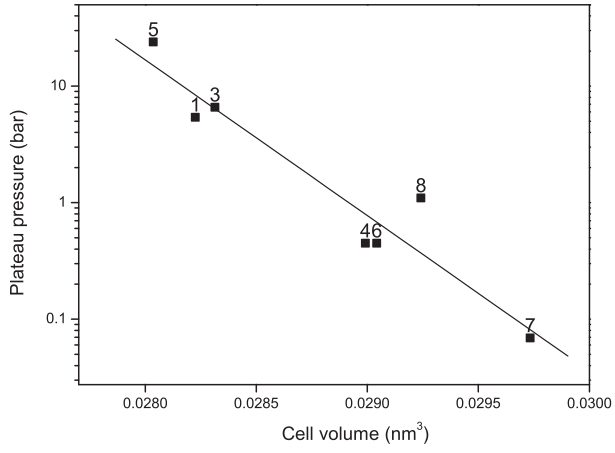

Fig. 6. Desorption plateau pressure at 100 °C as a function of the hydrogen-free bcc unit cell volume of the studied samples. Numbers refer to the sample no. as defined in Table 1 (maximum error bars: $\pm 0.12 \times 10^{-3}$ nm^3 and ±0.1 bar).

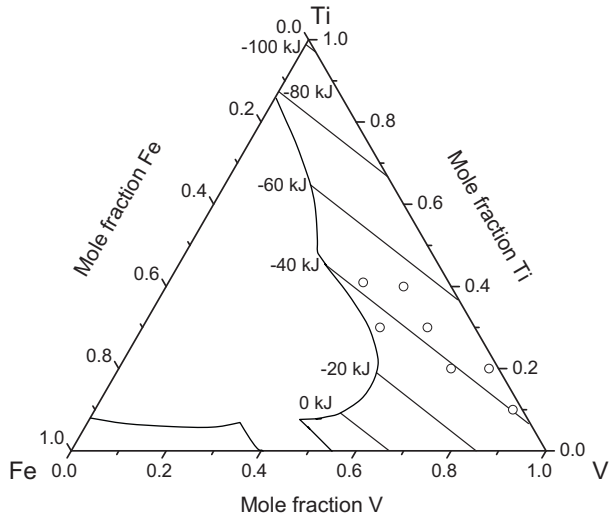

Fig. 7. Isocontour lines representing the enthalpy of formation of the fcc hydride obtained by the hydrogenation of bcc alloys in the Fe–Ti–V ternary system drawn in the Gibbs triangle. The lines, calculated with Eq. (3), are super-imposed to the extension of the bcc phase at 1200 °C (see Ref. [28]). The compositions studied in the present work are shown.

Table 5
Comparison of the desorption enthalpies obtained for pure elements (values refer to reactions TiH to TiH_2 [39], VH to VH_2 [26] and Fe to $FeH_{0.5}$ [39]) and calculated using Eq. (4) for the Fe–Ti–V ternary system.

	Ti	V	Fe
Enthalpy calculated from Eq. (4) (kJ mol$(H_2)^{-1}$)	117	38	−80
Enthalpy of pure elements (kJ mol$(H_2)^{-1}$)	136	40	−20

As far as hydrogen maximal capacities are concerned, a decrease is observed for an increasing iron content which can be better visualized in Fig. 8. The isocontour enthalpy and capacity lines are not strictly parallel. This is mainly because Ti and V have very different hydride formation enthalpies while they have similar absorption capacities. This means that, at a constant iron concentration, the enthalpy will change drastically as a function of Ti/V ratio, but not the capacity. This feature opens the possibility to find an optimum absorption capacity for a given hydride stability imposed by a given application.

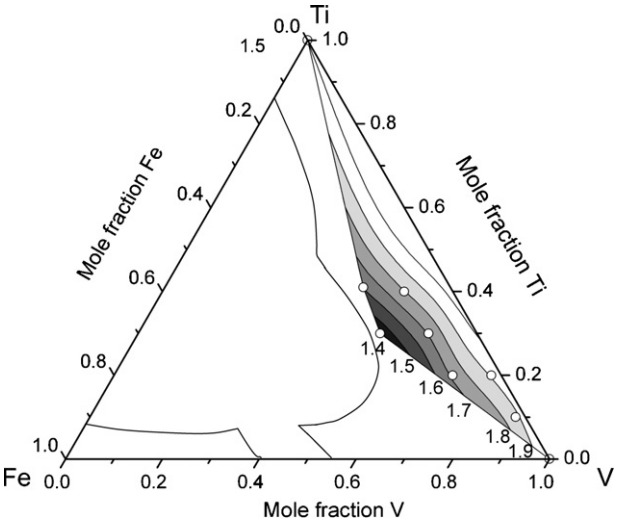

Fig. 8. Isocontour lines representing the maximum absorption capacity of the bcc alloys in the Fe–Ti–V ternary system drawn in the Gibbs triangle. The lines are calculated by interpolation between the values obtained for the different compositions studied shown as points. They are super-imposed to the extension of the bcc phase at 1200 °C (see Ref. [28]).

For each sample presented in Table 4, the pressure plateau width lies between 0.38 and 0.83 H/M. This plateau width, which is considered as a relevant parameter for the reversible capacity, is plotted as a function of the iron and vanadium concentrations in Fig. 9a and b, respectively. It can be seen that both an increase of the vanadium rate and a decrease of the iron rate result in an increase of the plateau width.

No tangible relationship could be observed between the hysteresis factor or the slope of the plateaus and the metallic composition, the lattice parameter or the electron-to-atom ratio.

As concerns the continuous bcc to bct transformation, it can be compared to the literature data for other systems. At low temperature, for the pure vanadium, there is a coexistence of the bcc and bct phases between 0.05 and 0.5 H/M. Above 200 °C, a continuous hydrogen enrichment of the bcc phase is observed for hydrogen concentrations smaller than 1 H/M [40]. Libowitz et al. [25] have reported at room temperature the presence of a single bcc phase for concentrations higher than 0.4 H/M for Ti–V alloys containing more than 10 at.% titanium. The transformation observed for the sample of composition $Ti_{20}V_{70}Fe_{10}$ has never been observed until now, and is an intermediate behavior between what was observed at room temperature for pure vanadium and for Ti–V alloys.

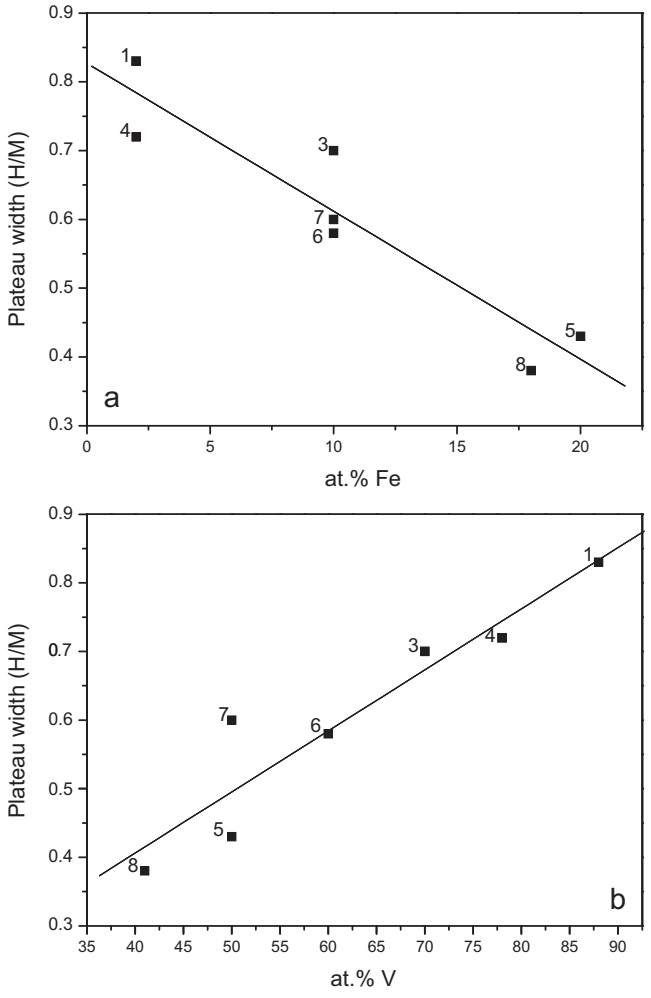

Fig. 9. Plateau width as a function of the iron rate (a) and of the vanadium rate (b) in the hydrogen-free samples. Numbers refer to the sample no. as defined in Table 1 (maximum error bars: ±0.1 H/M and ±3 at.%).

5. Conclusions

In the present work, the hydrogenation properties of ten Fe–Ti–V samples have been studied. The pressure–composition isotherms of seven samples have been measured at different temperatures. With these data, linear equations modeling the variation of the enthalpies of formation/dissociation of the hydride as a function of the composition of the bcc alloy have been established. Addition of iron destabilizes the hydride, while addition of titanium stabilizes it, which agrees with the literature data. An increase of the isotherm plateau width with increasing vanadium content and with decreasing iron content was also observed.

A study of the structure of the alloy of composition $Ti_{20}V_{70}Fe_{10}$ upon hydrogen absorption was carried out, showing that between 0 and ≈1 H/M, the crystallographic cell adopts a single phase bct structure increasing continuously, and then transforms discontinuously between ≈1 and ≈2 H/M from the bct to the fcc structure. This is the first time that such a behavior is reported for low hydrogen concentrations.

Acknowledgments

The authors would like to thank Dr. É. Leroy for EPMA analyses, and Dr. A. Lima and Veolia Environment for financial support.

References

[1] J.J. Reilly, R.H. Wiswall Jr., Inorg. Chem. 9 (7) (1970) 1678–1682.
[2] G.G. Libowitz, A.J. Maeland, Mater. Sci. Forum 31 (1988) 177–196.
[3] E. Akiba, M. Okada, MRS Bull. 27 (2) (2002) 699–703.
[4] A.J. Maeland, G.G. Libowitz, J.P. Lynch, J. Less-Common Met. 104 (2) (1984) 361–364.
[5] S.W. Cho, C.S. Han, C.N. Park, E. Akiba, J. Alloys Compd. 288 (1999) 294–298.
[6] T. Tamura, A. Kamegawa, H. Takamura, M. Okada, Mater. Trans. JIM 42 (9) (2001) 1862–1865.
[7] H. Itoh, H. Arashima, K. Kubo, T. Kabutomori, J. Alloys Compd. 330–332 (2002) 287–291.
[8] M. Okada, T. Kuriiwa, T. Tamura, H. Takamura, A. Kamegawa, J. Alloys Compd. 330–332 (2002) 511–516.
[9] K. Shirasaki, T. Tamura, T. Kuriiwa, T. Goto, A. Kamegawa, H. Takamura, M. Okada, Mater. Trans. JIM 43 (5) (2002) 1115–1119.
[10] S.-W. Cho, C.-N. Park, J.-H. Yoo, J. Choi, J.-S. Park, C.-Y. Suh, G. Shim, J. Alloys Compd. 403 (1–2) (2005) 262–266.
[11] H. Pan, R. Li, M. Gao, Y. Liu, Q. Wang, J. Alloys Compd. 404–406 (2005) 669–674.
[12] X.B. Yu, J.Z. Chen, Z. Wu, B.J. Xia, N.X. Xu, Int. J. Hydrogen Energy 29 (13) (2004) 1377–1381.
[13] J. Chen, C.C. Chuang, K. Hong, Proceedings of the Advances in Hydrogen Energy 10th World Hydrogen Energy Conference, Cocoa Beach, 1994, pp. 1089–1098.
[14] K. Nomura, E. Akiba, J. Alloys Compd. 231 (1995) 513–517.
[15] Y. Nakamura, E. Akiba, J. Alloys Compd. 311 (2000) 317–321.
[16] X.B. Yu, S.L. Feng, Z. Wu, B.J. Xia, N.X. Xu, J. Alloys Compd. 393 (1–2) (2005) 128–134.
[17] G. Sandrock, J. Alloys Compd. 293–295 (1999) 877–888.
[18] J.F. Lynch, A.J. Maeland, G.G. Libowitz, Z. Phys. Chem. Neue Folge 145 (1985) 51–59.
[19] X.B. Yu, Z.X. Yang, S.L. Feng, Z. Wu, N.X. Xu, Int. J. Hydrogen Energy 31 (9) (2006) 1176–1181.
[20] J.H. Yoo, G. Shim, S.W. Cho, C.N. Park, Int. J. Hydrogen Energy 32 (14) (2007) 2977–2981.
[21] H. Liang, Y. Chen, Y. Yan, C. Wu, M. Tao, Mater. Sci. Eng. A 448 (2007) 128–134.
[22] Z. Huang, F. Cuevas, X.P. Liu, M. Latroche, J. Du, Int. J. Hydrogen Energy 34 (2009) 9385–9392.
[23] A.J. Maeland, G.G. Libowitz, J.F. Lynch, G. Rak, J. Less-Common Met. 104 (1984) 133–139.
[24] J.F. Lynch, A.J. Maeland, G.G. Libowitz, Proc. of the 5th World Hydrogen Energy Conference, Toronto, Canada, 1984, pp. 1327–1337.
[25] G.G. Libowitz, A.J. Maeland, J.F. Lynch, Final Report, Brookhaven National Laboratory, Upton, Long Island, 1985.
[26] A.O. Kagawa, E. Kusakabe, T.Y. Sakamoto, J. Less-Common Met. 172–174 (1991) 64–70.
[27] S. Challet, M. Latroche, F. Heurtaux, J. Alloys Compd. 439 (1–2) (2007) 294–301.
[28] B. Massicot, J.-M. Joubert, M. Latroche, The Fe–Ti–V system, Int. J. Mater. Res., available on line at http://www.ijmr.de/ijmr/o_archiv.asp?ps=MK110379&task=03&o_id=25112811648-50, in press.
[29] H.M. Rietveld, J. Appl. Crystallogr. 2 (1969) 65–71.
[30] J. Rodríguez-Carvajal, Physica B 192 (1993) 55–69.
[31] J.F. Bérar, Data Optimization Propagation of Errors in Powder Diffraction, NIST Special Publication, 1992, pp. 63–67.
[32] J.F. Bérar, P. Lelann, J. Appl. Crystallogr. 24 (1991) 1–5.
[33] A. Guéguen, J.-M. Joubert, M. Latroche, Influence of the C14 Ti33V33Fe33 Laves phase on the hydrogenation properties of the body-centered cubic compound Ti24.5V59.3Fe16.2., J. Alloys Compd., submitted for publication.
[34] A. Sieverts, Z. Phys. Chem. 60 (1907) 129–201.
[35] Y. Noda, K. Masumoto, K. Koike, S. Suzuki, S. Sato, Acta Crystallogr. B 42 (6) (1986) 529–533.
[36] T. Kajitani, M. Hirabayashi, Z. Phys. Chem. Neue Folge 145 (1985) 27–42.
[37] K. Asano, M. Hirabayashi, Interstitial superstructures of vanadium deuterides, Phys. Status Solidi (a) 15 (1) (1973) 267–279.
[38] M. Latroche, J. Phys. Chem. Sol. 65 (2004) 517–522.
[39] R. Griessen, T. Riesterer, Heat of formation models, in: L. Schlapbach (Ed.), Hydrogen in Intermetallic Compounds. I. Electronic, Thermodynamic, and Crystallographic Properties, Preparation, Springer-Verlag, Berlin, 1988, pp. 219–284.
[40] C.H. Fagerstroem, F.D. Manchester, J.M. Pitre, in: D. Manchester (Ed.), Phase Diagrams of Binary Hydrogen Alloys, ASM International, 2000, pp. 273–292.